Materials Chemistry and Physics 162 (2015) 659–670

Contents lists available at ScienceDirect

Materials Chemistry and Physics

journal homepage: www.elsevier.com/locate/matchemphys

Diffusion behavior of *Cr* diluted in bcc and fcc *Fe*: Classical and quantum simulation methods

Viviana P. Ramunni [a, b, *], Alejandro M.F. Rivas [a, c]

[a] CONICET, Avda. Rivadavia 1917, Cdad. de Buenos Aires C.P. 1033, Argentina
[b] Comisión Nacional de Energía Atómica, Gerencia Materiales, Av. Del Libertador 8250, C1429BNP Ciudad de Buenos Aires, Argentina
[c] Comisión Nacional de Energía Atómica, Departamento de Física Teórica, Tandar, Av. Del Libertador 8250, C1429BNP Ciudad de Buenos Aires, Argentina

HIGHLIGHTS

- Comparison of diffusion coefficients obtained from classical and quantum methods.
- We perform our calculations in diluted bcc/fcc Fe–Cr alloy.
- Magnetic and phonon effects must be taken into account.
- Classical calculations are in perfect agreement with experimental data.

GRAPHICAL ABSTRACT

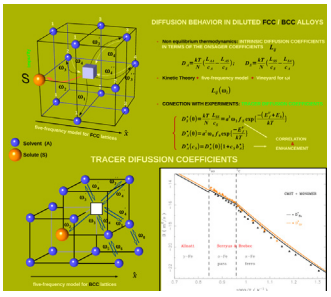

ARTICLE INFO

Article history:
Received 10 October 2014
Received in revised form
2 June 2015
Accepted 18 June 2015
Available online 2 July 2015

Keywords:
Diffusion
Computational techniques
Molecular dynamics
ab initio calculations
Alloys
Thermodynamic properties
Transport properties

ABSTRACT

We characterize the atomic mobility behavior driven by vacancies, in bcc and fcc *Fe–Cr* diluted alloys, using a multi-frequency model. We calculate the full set of the Onsager coefficients and the tracer self and solute diffusion coefficients in terms of the mean jump frequencies. The involved jump frequencies are calculated using a classical molecular static (CMS) technique. For the bcc case, we also perform quantum calculations based on the density functional theory (DFT). There, we show that, in accordance with Bohr's correspondence principle, as the size of the atomic cell (total number of atoms) is increased, quantum results with DFT recover the classical ones obtained with CMS calculations. This last ones, are in perfect agreement with available experimental data for both, solute and solvent diffusion coefficients. For high temperatures, in the fcc phase where no experimental data are yet available, our CMS calculations predict the expected solute and solvent diffusion coefficients.

1. Introduction

Recently, Hurtado et al. [1] have studied the hydrogen (*H*) diffusion effect on 9*Cr* steels, revealing a permeation coefficient 10 times lower and a diffusion coefficient 200 times lower than in pure annealed iron. Also, based on the numerical resolution of Fick's equations in presence of trapping sites in comparison with electrochemical *H* detection curves, Castaño et al. [2] provided quantitative information about the binding energy between *H* and trapping sites during the *H* diffusion process [1]. Ferritic or martensitic steels with *Cr* are presently used in conventional supercritical thermal power plants and are candidates for future IV

* Corresponding author. CONICET, Avda. Rivadavia 1917, Cdad. de Buenos Aires C.P. 1033, Argentina.
E-mail address: vpram@cnea.gov.ar (V.P. Ramunni).

http://dx.doi.org/10.1016/j.matchemphys.2015.06.040
0254-0584/

generation supercritical water cooled nuclear reactors.

Furthermore, it is imperative to explore the modeling of *H* trapping sites and possible migration paths that can explain the experimental observations. However, before dealing with modeling *H* traps, it is important to carefully study the initial microscopic processes that can delay the *H* atoms during diffusion. With that purpose in mind, as the 9*Cr* martensitic steel of BCT structure is a complex system to be simulated, we must firstly understand the diffusion process for simpler structures. Hence, in this work we study numerically the static and dynamical properties of vacancies in both, a bcc (or ferritic) and fcc *Fe*−*Cr* matrix.

In the linear response framework the diffusion coefficients, as was early shown [3,5], can be entirely expressed in terms of the commonly known Onsager coefficients L_{ij}. The L_{ij} are the fundamental kinetic quantities. In the context of the commonly known as multi-frequency model, originally developed by Le Claire [6], the Onsager coefficients for vacancy mediated diffusion can in turn be expressed in terms of frequency jumps rates of various atom-vacancy exchanges relative to a solute atom.

Recently, attends were made in order to describe the diffusion process by obtaining numerically the needed jump frequencies. However, disagreement between the experimental and ad-initio based DFT calculated, diffusion coefficients where observed in [8] for *Ni*−*Cr* and *Ni*−*Fe* bcc alloys. Similarly, but for fcc structures, DFT calculations performed by Mantina et al. [9] for *Mg*, *Si* and *Cu* diluted in *Al*, obtained again numerical results that do not correctly describe the experimental data.

For the particular case of *Fe* based diluted alloys, in a recent work, Choudhury et al. [5] have performed an ab-initio based calculation of the self-diffusion and solute diffusion coefficients for diluted α*Fe*−*Ni* and α*Fe*−*Cr* alloys, using the Vienna ab-initio Simulation Package (VASP). It is shown in [5], that the slope of the ab-initio based diffusion coefficients as a function of inverse temperature (i.e. the activation barrier) matches well with experimental measurements, for both the para- and ferro-magnetic orders considered. However, the absolute value of the DFT calculated diffusion coefficients differs in four orders of magnitudes from experimental measurements.

Also, Martínez et al. [4], have calculated the tracer diffusion coefficient in *Fe*−*Cr* diluted alloys, using classical atomistic kinetic Monte Carlo pair interactions, and taking into account entropic contributions to the vacancy formation and migration energies. Then, the obtained results accurately reproduces the experimental data.

On the other hand, employing classical molecular statics (CMS) technique, in order to obtain the needed frequency jumps, one of us has presented studies of impurity diffusion behavior in Nickel-Aluminium and Aluminium-Uranium fcc diluted alloys [3]. It is then shown that all the diffusion coefficients obtained with CMS are in good agreement with experimental data for both alloys. Hence, CMS is appropriate in order to describe the impurity diffusion behavior mediated by a vacancy mechanism.

In the present work, we characterize the diffusion behavior in *Fe*−*Cr* diluted alloys in an important temperature range that includes both para and ferro magnetic orders as well as bcc and fcc lattice structures. For the multi frequency models, we have used the model of Serruys and Brevec [7] for bcc *Fe* and the model of Allnatt [10,11] for fcc *Fe*.

For the bcc phase, we have performed our calculations using both, CMS as well DFT calculations. We have compared the obtained diffusion coefficients including and excluding several factors. In particular, the explicit calculation of phonon spectrum, or equivalently migration entropic effects, in order to compute the mean jump frequencies, as well as, magnetic corrections for the ferromagnetic phase. DFT calculations have been performed with 54 and 128 atoms. All this calculations have been compared with experimental data when available.

We show here that, CMS calculations of the diffusion coefficients are in perfect agreement with experimental data, when we include both the explicit calculation of phonon spectrum and magnetic corrections. Meanwhile for DFT calculations we find that, in accordance with Bohr's correspondence principle, as the size of the atomic cell (total number of atoms) is increased the quantum results with DFT, recover the classical ones obtained with CMS.

At this respect, we must not expect to observe quantum effects for such macroscopic systems even more for the high temperatures here described. In that case, the interaction of the system with the thermal environment implies in decoherence effects, where the classical limit is expected to be recovered. It must be also noted that CMS simulations are much less computationally expensive method than DFT. For which computational time largely increases with the number of atoms of the quantum sample to be simulated.

For the higher temperature fcc phase of *Fe*−*Cr*, we have performed CMS calculations of the diffusion coefficients. In that case there is no experimental data available yet. Diffusion plays an important role in the kinetics of many materials processes. Experimental measurements of diffusion coefficients are expensive, difficult and in some cases nearly impossible. A complimentary approach is to determine diffusivities in materials by atomistic computer simulations. For the *Fe*−*Cr* fcc phase, our CMS calculations predicts the diffusion behavior.

In addition to predicting diffusion coefficients, computer simulations can provide insights into atomic mechanisms of diffusion processes, creating a fundamental framework for materials design strategies. At this respect, we show here that, in accordance with Choudhury et al. [5] for the bcc *Fe* case, a vacancy drag mechanism is unlikely to occur in bcc as well as in fcc *Fe*−*Cr*.

We have summarized the theoretical tools needed to express the diffusion coefficients in terms of microscopic magnitudes such as, the jump frequencies, the free vacancy formation energy and the vacancy-solute binding energy. We start with non-equilibrium thermodynamics in order to relate the diffusion coefficients with the phenomenological Onsager *L*-coefficients in both, bcc and fcc structures. Then, the microscopic kinetic theory, allows us to write the Onsager coefficients in term of the jump frequency rates [7,10,11], which are evaluated from the migration barriers and the phonon frequencies under the harmonic approximation. The attempt jump frequencies are obtained from the migrations barriers within the conventional framework by Vineyard [12] that corresponds to the classical limit. In order to compute the saddle points configurations, from which we obtain the jumps frequencies defined in the multi-frequency model, we employ the economic Monomer method [13] (previously used in Refs. [3,14–16]). Note that, the Monomer method coupled to CMS simulations is a much less computationally expensive method, that allows us to compute at low cost a bunch of jump frequencies from which we can perform averages in order to obtain more accurate effective frequencies.

The paper is organized as follows. In Section 2 we briefly introduce a summary of the macroscopic equations of atomic transport that are provided by non-equilibrium thermodynamics [17,18]. In this way analytical expressions of the tracer diffusion coefficients in binary alloys, in terms of Onsager coefficients, are presented. In Section 3, for diffusion mediated by a vacancy mechanism, we briefly introduce the full set of the Onsager coefficients calculated by Allnatt and Serryus and Brevec [7,10,11], in terms of jumps frequencies, in the second-nearest neighbor binding model for fcc/bcc lattices respectively. In Section 4, we present the way to evaluate the tracer diffusion coefficients in diluted binary alloys in terms of the Onsager coefficients. This procedure allows to express the diffusion coefficients in terms of the

frequency jumps. Section 5, is devoted to present our numerical results using the theoretical procedure previously summarized and making a comparison with available experimental data. The last section briefly presents some conclusions.

2. The flux equations

Isothermal atomic diffusion can be described through a linear expression between the fluxes, $\mathbf{J}_k$, and the driving forces, $\mathbf{X}_k$, related by the Onsager coefficients L_{ij} as,

$$\mathbf{J}_k = \sum_i^N L_{ki}\mathbf{X}_i, \tag{1}$$

where N is the number of components in the system, $\mathbf{J}_k$ describes the flux vector density of component k, while $\mathbf{X}_k$ is the driving force acting on component k. The second range tensor L_{ij} is symmetric ($L_{ij} = L_{ji}$) and depends on pressure and temperature, but is independent of the driving forces $\mathbf{X}_k$. On the other hand, for each k component, the driving forces may be expressed, in absence of external force, in terms of the chemical potential μ_k, so that,

$$\mathrm{X}_k = -T\nabla\left(\frac{\mu_k}{T}\right). \tag{2}$$

In (2) T is the absolute temperature, and the chemical potential, μ_k, is the partial derivative of the Gibbs free energy with respect to the number of atoms of specie k,

$$\mu_k = \left(\frac{\partial G}{\partial N_k}\right)_{T,P,N_{j\neq k}} = \mu_k^{\circ}(T,P) + k_BT\ln(C_k\gamma_k), \tag{3}$$

where γ_k is the activity coefficient, which is defined in terms of the activity $a_k = \gamma_k C_k$ and the molar concentration of specie k, C_k.

For the particular case of a binary alloy with N available lattice sites per unit volume, containing molar concentrations C_A for host atoms A, C_S of solute atoms S (impurities), the fluxes in terms of the Onsager coefficients are expressed as,

$$\mathbf{J}_A = -\frac{k_BT}{N}\left(\frac{L_{AA}}{C_A} - \frac{L_{AS}}{C_S}\right)\left(1 + \frac{\partial\ln\gamma_A}{\partial\ln C_A}\right)\nabla C_A, \tag{4}$$

$$\mathbf{J}_S = -\frac{k_BT}{N}\left(\frac{L_{SS}}{C_S} - \frac{L_{AS}}{C_A}\right)\left(1 + \frac{\partial\ln\gamma_S}{\partial\ln C_S}\right)\nabla C_S, \tag{5}$$

with

$$\mathbf{J}_V = -\mathbf{J}_A - \mathbf{J}_S, \tag{6}$$

for the flux of vacancies. From (4) and (5), the intrinsic diffusion coefficients for solvent A and solute S, are respectively defined as

$$D_A = \frac{k_BT}{N}\left(\frac{L_{AA}}{C_A} - \frac{L_{AS}}{C_S}\right)\phi_A, \tag{7}$$

and

$$D_S = \frac{k_BT}{N}\left(\frac{L_{SS}}{C_S} - \frac{L_{SA}}{C_A}\right)\phi_S. \tag{8}$$

In Eqs. (7) and (8), the quantities ϕ_A, ϕ_S are known as the thermodynamical factors,

$$\phi_A = \left(1 + \frac{\partial\ln\gamma_A}{\partial\ln C_A}\right) = \phi_S = \left(1 + \frac{\partial\ln\gamma_S}{\partial\ln C_S}\right). \tag{9}$$

In the dilute limit, the thermodynamics factor $\phi_A = \phi_S = 1$, which simplifies the expression of the tracer diffusion coefficients in terms of the phenomenological coefficients.

The standard intrinsic diffusion coefficients in Eqs. (7) and (8) can be expressed in terms of the tracer solute diffusion coefficients $D_A^{\star}$ and $D_S^{\star}$ which are measurable quantities, and the collective correlation factor f_{ij} ($i, j = A, S$) [18,19] as

$$D_A = D_A^0\left[f_{AA} - \frac{C_A}{C_S}f_{AS}^{(A)}\right]\phi_A = D_A^{\star}\left[\frac{f_{AA}}{f_A} - \left(\frac{C_A}{C_S}\right)\frac{f_{AS}^{(A)}}{f_A}\right]\phi_A, \tag{10}$$

$$D_S = D_S^0\left[f_{SS} - \frac{C_S}{C_A}f_{AS}^{(S)}\right]\phi_S = D_S^{\star}\left[\frac{f_{SS}}{f_S} - \left(\frac{C_S}{C_A}\right)\frac{f_{AS}^{(S)}}{f_S}\right]\phi_S. \tag{11}$$

The intrinsic diffusion coefficients in (10) and (11) are known as the modified Darken equations, where $D_S^0 = s^2\Gamma_i/6$ is the diffusion coefficients of atoms of the tracer S in a complete random walk performing Γ_i jumps of length s per unit time. The collective correlation factors f_{ij} are related to the L_{ij} coefficients through,

$$f_{AA} = \frac{k_BT}{NC_A}L_{AA}\left(\frac{1}{D_A^0}\right)\ ;\ f_{SS} = \frac{k_BT}{NC_S}L_{SS}\left(\frac{1}{D_S^0}\right), \tag{12}$$

and for the mixed terms,

$$f_{AS}^{(A)} = \frac{k_BT}{NC_A}L_{AS}^{(A)}\left(\frac{1}{D_A^0}\right)\ ;\ f_{AS}^{(S)} = \frac{k_BT}{NC_S}L_{AS}^{(S)}\left(\frac{1}{D_S^0}\right). \tag{13}$$

The tracer correlation factors f_A, f_S are defined as the ratios $f_A = D_A^{\star}/D_A^0$ and $f_S = D_S^{\star}/D_S^0$ respectively. The term in square brackets in the second term of equations (10) and (11), is the vacancy wind factor G [20].

In the next sections, we present the Onsager coefficients in terms of the atomic jump frequencies taken from Refs. [7,10,11].

3. The phenomenological Onsager coefficients for bcc and fcc lattices

Present calculations are focused on the transport phenomena of binary alloys, specifically on the corresponding transport coefficients and how these are related to microscopical magnitudes. In this way, Serryus and Brevec [7], for bcc lattices, and Allnatt [10,11], for fcc ones, gave compact expressions for the L– coefficients by treating the contribution of the vacancy-impurity exchanges in terms of the atomic jump frequencies. Hence we treat here the case of binary alloys with a host specie A with a concentration C_A and solute S with a concentration C_S. In the model here described the migration is mediated by a vacancy mechanism. The concentration of vacancies is C_V and in particular there is a concentration C_p of vacancies that are at first neighbor with a solute atom.

3.1. The Onsager equations for bcc lattices

We adopt an effective multi-frequency model à la Le Claire [6], assuming that the perturbation of the solute movement by a vacancy V, is limited to its immediate vicinity. Fig. 1 defines the jump rates ω_i (i = 0, 1, 2, 3, 4, 5, 6) considering only jumps between neighbors.

For them, w_2 implies in the exchange between the vacancy and the solute. The frequency of jumps such that the vacancy goes to sites that are second neighbor of the solute is denoted by ω_3. The model includes the jump rate ω_4 for the inverse of ω_3. Jumps toward sites that are third and forth neighbor of the solute are all denoted

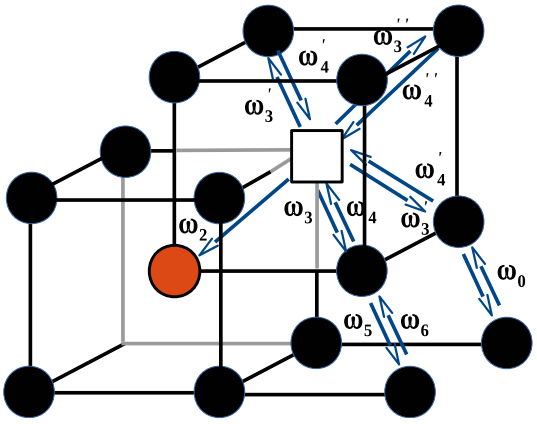

Fig. 1. The frequencies involved in the second binding model for bcc lattices. In black/orange circles, respectively are represented the solvent and solute atoms. (For interpretation of the references to colour in this figure legend, the reader is referred to the web version of this article.)

with ω_3' and ω_3'' respectively while ω_4' and ω_4'' are used for their respective inverse frequency jumps. Jumps from the second neighbor of the solute are denoted by ω_5, while ω_6 is used for the respective reverse jumps. The jump rate ω_0 is used for vacancy jumps among sites more distant than the fifth neighbor site.

As was shown in Refs. [7], the full set of the Onsager coefficients can be written as [5],

$$L_{AA} = \frac{a^2\omega_0 N \exp\left(-E_f^V/k_BT\right)}{k_BT}(1 + b_A C_S), \tag{14}$$

$$L_{AS} = L_{SA} = \frac{2a^2\omega_2 \exp\left(-E_f^V/k_BT\right)}{k_BT}\left(\frac{\omega_4}{\omega_3}\right)\exp\left(-E_m^V/k_BT\right) \tag{15}$$

$$\times\frac{n_S}{\psi}\left[\frac{(8u-7)B_2 - 32(u^2-1)B_1}{4u(u+1)B_3}\right], \tag{16}$$

$$L_{SS} = \frac{a^2\omega_2 \exp\left(-E_f^V/k_BT\right)}{k_BT}\exp\left(-E_m^V/k_BT\right) \tag{17}$$

$$\times\frac{n_S}{\psi}\left[\frac{(8u+7)B_2 - 32u(u+1)B_1}{4u(u+1)B_3}\right], \tag{18}$$

where E_f^V and E_m^V denotes the vacancy formation and migration energies respectively and a is the bcc solvent lattice parameter. The remaining coefficients are expressed as

$$B_1 = 8u^2 + 77u + 155, \tag{19}$$

$$B_2 = 32u^3 + 324u^2 + 810u + 475, \tag{20}$$

$$B_3 = \frac{(2v + 8u + 7)B_6 - 32u(u+1)B_5}{4u(u+1)} \tag{21}$$

$$B_5 = 8u^2 + 77u + 155 \tag{22}$$

$$B_6 = 32u^3 + 324u^2 + 810u + 475 \tag{23}$$

$$B_7 = \frac{(2v + 8u + 7)B_6 - 32u(u+1)B_5}{4u(u+1)} \tag{24}$$

$$\psi = 1 + \left(50 + \frac{8\omega_4^\star}{\omega_3^\star}\right)\exp\left(-E_f^V/k_BT\right), \tag{25}$$

in terms of the ratios $u = \omega_4^\star/\omega_0$, $v = \omega_2/\omega_3^\star$ with the effective frequencies $\omega_3^\star$ and $\omega_4^\star$ defined from Fig. 1 and Ref. [5] as,

$$7\omega_3^\star = 3\omega_3 + 3\omega_3' + \omega_3'', \tag{26}$$

and

$$7\omega_4^\star = 3\omega_4 + 3\omega_4' + \omega_4''. \tag{27}$$

The term b_A in (14) is usually called as the solvent enhancement factor,

$$b_A = -58 + \frac{1}{\psi}\left\{45 + 12u + \frac{6u + 2v(u-1) - 7}{u} \times\left[\frac{(8u-7)B_6}{2(u+1)B_7} - 16(u-1)\frac{B_5}{B_7}\right]\right\}. \tag{28}$$

Finally, from L_{ss} in (18), we can define the solute correlation factor,

$$f_S = \frac{7\omega_3^\star F}{2\omega_2 + 7\omega_3^\star F}, \tag{29}$$

where the F factor in (29) is calculated from,

$$7F = \frac{3u^3 + \xi_1 u^2 + \xi_2 u + \xi_3}{u^3 + \xi_4 u^2 + \xi_5 u + \xi_6}, \tag{30}$$

and the constants ξ_n in (30), are summarized in Table 1.

3.2. The Onsager equations for fcc lattices

The description of the jumps in Fig. 2 is similar to that in Fig. 1. Now, we include w_1, when the exchange between the vacancy and the solvent atom lets the vacancy as a first neighbor to the solute.

As was shown in Refs. [10,11], the Onsager coefficient for the solute specie in terms of the mean jump frequencies in Fig. 2, can be written as

$$L_{SS} = L(\omega_2)\left\{1 - \frac{2\omega_2}{\Omega}\right\} = L(\omega_2)f_S \tag{31}$$

were f_S is called the tracer correlation factor for the solute and the function $L(\omega_i)$ is,

$$L(\omega_i) = \frac{a^2}{12}N\beta C_p\omega_i. \tag{32}$$

In (32) a is the lattice parameter for fcc solvent A, and C_p denotes the site fraction of solute atoms with a vacancy among their z nearest-neighbor sites. Ω in (31) is given by

Table 1
Numerical constants ξ_n for the second-nearest-neighbor binding model taken from Ref. [7].

	ξ_1	ξ_2	ξ_3	ξ_4	ξ_5	ξ_6
Ref. [7]	41.37	140.94	103.91	10.13	25.31	14.84

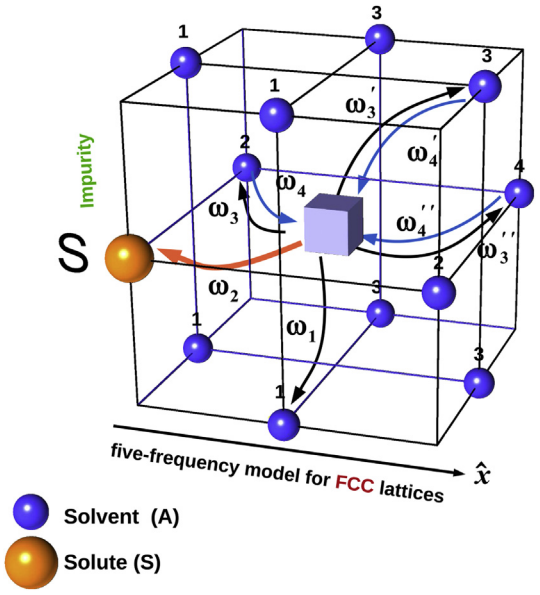

Fig. 2. The multi-frequency model for fcc lattices.

$$\Omega = 2(\omega_1 + \omega_2) + 7\omega_3^{\star} F. \tag{33}$$

Inserting the expression (33) for Ω in (31), we get for the tracer correlation factor for the solute,

$$f_S = \frac{2\omega_1 + 7\omega_3^{\star} F}{2(\omega_1 + \omega_2) + 7\omega_3^{\star} F}. \tag{34}$$

The quantity F in (34) is a function of the ratio $u = \omega_4^{\star}/\omega_0$ which is expressed as,

$$7(1-F) = \frac{u(\xi_1 u^3 + \xi_2 u^2 + \xi_3 u + \xi_4)}{\xi_5 u^4 + \xi_6 u^3 + \xi_7 u^2 + \xi_8 u + \xi_9}. \tag{35}$$

The ξ_i coefficients in (35) are shown in Table 2, they were calculated by Koiwa [21] using perturbative methods. In the fcc case, we express effectives mean jump frequencies as in Ref. [5],

$$7\omega_3^{\star} = 2\omega_3 + 4\omega_3' + \omega_3'', \tag{36}$$

and

$$7\omega_4^{\star} = 2\omega_4 + 4\omega_4' + \omega_4''. \tag{37}$$

Also according with [10,11], the mixed coefficient L_{AS} is,

$$L_{AS} = L_{SA} = 2L(\omega_2) \times \left\{ 3\omega_3^{\star} - 2\omega_1 + 7\omega_3^{\star}(1-F)\left(\frac{\omega_0 - \omega_4^{\star}}{\omega_4^{\star}}\right)\right\} \frac{1}{\Omega}. \tag{38}$$

While for the solvent,

Table 2
Coefficients in the expression for F for the five frequency model calculated by Koiwa [21].

	ξ_1	ξ_2	ξ_3	ξ_4	ξ_5	ξ_6	ξ_7	ξ_8	ξ_9
Ref. [21]	10	180	924	1338	2	40	253	596	435

$$L_{AA} = L_{AA}^{(0)} + L_{AA}^{(1)} \tag{39}$$

with

$$L_{AA}^{(0)} = L(4\omega_1 + 14\omega_3^{\star}) + 2N\beta s^2 \omega_0 (C_V - C_p)\left[1 - 7(C_S - C_p)\right], \tag{40}$$

and

$$\begin{aligned} L_{AA}^{(1)} = &-2L(3\omega_3^{\star} - 2\omega_1)\left[(3\omega_3^{\star} - 2\omega_1) + 7\omega_3^{\star}(1-F)\left(\frac{\omega_0 - \omega_4^{\star}}{\omega_4^{\star}}\right)\right]\frac{1}{\Omega} \\ &-2L(3\omega_3^{\star} - 2\omega_1) \times \left[7\omega_3^{\star}(1-F)\left(\frac{\omega_0 - \omega_4^{\star}}{\omega_4^{\star}}\right)\right]\frac{1}{\Omega} \\ &-2L(3\omega_3^{\star})\left(\frac{\omega_0 - \omega_4^{\star}}{\omega_4^{\star}}\right)^2 \times \left[7(1-F)(2\omega_2 + 2\omega_1 + 7\omega_3^{\star})\frac{1}{\Omega}\right]. \end{aligned} \tag{41}$$

In order to evaluate the L-coefficients (31), (38) and (39), two parameters are needed, namely, the fraction of unbounded vacancies $C_V' = C_V - C_p$ and the unbound solute atoms $C_S' = C_S - C_p$. They are related with the frequency jumps through the mass action equation [6],

$$\frac{C_p}{C_V' C_S'} = z \exp(-E_b/k_B T) = \frac{\omega_4^{\star}}{\omega_3^{\star}}, \tag{42}$$

where E_b is the binding energy of the solute atom with a vacancy at its nearest neighbor sites and $z = 12$ is the coordination number for fcc lattices. Then, if the pairs and free vacancies are in local equilibrium and the fraction of solute C_S is much greater than both C_V and C_p, we can define the equilibrium constant K as,

$$\frac{C_p}{C_V - C_p} = zC_S \exp(-E_b/k_B T) \equiv KC_S, \tag{43}$$

and equivalently

$$C_p = C_V\left(\frac{KC_S}{1 + KC_S}\right). \tag{44}$$

3.3. From migration energies to frequency jumps

In order to compute the jump frequencies ω_i, we use the conventional treatment formulated by Vineyard [12], corresponding to the classical limit. In the classical description the vibrational prefactors of the mean jump frequencies do not depend on temperature, and has been conventionally used for evaluating the mean jump frequency as,

$$\omega_i = \nu_0^{\star} \exp\left(-E_m^i / k_B T\right). \tag{45}$$

with, the "attempt frequency"

$$\nu_0^{\star} = \frac{\prod_{i=1}^{3N-3} \nu_i^I}{\prod_{i=1}^{3N-4} \nu_i^S} = \nu_D \exp\left(\frac{S_m}{k_B}\right), \tag{46}$$

where E_m^i are the migration barriers calculated at $T = 0$ K. ν_i^I and ν_i^S are the frequencies of the normal vibrational modes at the initial and saddle points, respectively. In (46), the numerator refers to the

vibrational frequencies for the X–V pair (X = Fe,Cr) nearest neighbors in *Fe* matrix and the denominator to the saddle configuration for the *Fe*/*Cr*-vacancy exchange. For this last one, the product does not include the unstable mode. Note that, Eq (46) is based on calculation of the frequencies of the normal vibrational modes. This normal modes can involve only one atom or being collective modes. Alternatively, in the last expression, the "attempt frequency" can be expressed in terms of the Debye frequency ν_D and the migration entropy S_m.

Once the jump frequencies in the multi-frequency model have been computed, the diffusion coefficients are calculated using analytical expressions in terms of the temperature. It is important to note that in Ref. [22] it has been shown that there is discrepancy between the classical and the quantum calculations of $\nu_0^\star$. Although these discrepancies are large in the low-temperature range the quantum value gradually converges to the classical one at temperatures higher than room temperature [22]. Hence, here we employ a classical description.

4. The tracer diffusion coefficients for diluted alloys

Here, we focus on the self-diffusion and solute coefficients in a binary A–S alloy in the diluted limit. In this limit, $C_S \to 0$, the thermodynamics factor $\phi_A = \phi_S = 1$ and the intrinsic diffusion coefficient D_S in (8), is identical to the tracer diffusion coefficient $D_S^\star$,

$$D_S = D_S^\star(0) = \frac{k_B T}{N C_S} L_{SS}. \tag{47}$$

Introducing L_{SS} from (18) and (31) in (47), respectively for bcc and fcc lattices and assuming that $C_V \gg C_p$ and $C_V \gg C_p$ in (42), we obtain an expression for the tracer solute diffusion coefficient as,

$$D_S^\star = a^2 \omega_2 f_S C_V \left(\frac{\omega_4^\star}{\omega_3^\star}\right), \tag{48}$$

where f_S, the solute correlation, is expressed for bcc lattices as

$$f_S = \left\{\frac{7\omega_3^\star F}{2\omega_2 + 7\omega_3^\star F}\right\}, \tag{49}$$

while for fcc lattices as

$$f_S = \left\{\frac{2\omega_1 + 7\omega_3^\star F}{2(\omega_1 + \omega_2) + 7\omega_3^\star F}\right\}, \tag{50}$$

where the function F is given by expression (30) or (35), respectively for bcc or fcc structures.

At thermodynamic equilibrium the vacancy concentration C_V is given by,

$$C_V = \exp\left(-E_f^V \Big/ k_B T\right). \tag{51}$$

where E_f^V is the vacancy formation energy in pure A.

As in Ref. [8], the self-diffusion coefficient $D_A^\star(0)$ for pure A, can be obtained from the expression (48) for $D_S^\star$, by replacing all the jump frequencies ω_i by ω_0. Hence, the self-diffusion coefficient can be written as:

$$D_A^\star(0) = a^2 \omega_0 C_V f_0, \tag{52}$$

where f_0, the correlation factor for pure bcc or fcc metals, can be obtained directly from f_S, respectively in (49) or (50), by replacing all the jump frequencies ω_i by ω_0. Note that if we introduce the coefficients ξ_i in Tables 1 and 2 in respective equations of F, then we obtain $7F = 5.33$ and $7F = 5.15$, respectively for bcc and fcc lattices. Introducing $7F = 5.33$ in (49) and $7F = 5.15$ in (50), we get $f_0 = 0.7272/f_0 = 0.7814$, which correspond to the correlation factor in pure bcc and fcc metals respectively.

On the other hand, based on Le Claire's model [6], the tracer self-diffusion coefficient $D_A^\star(C_S)$ with a diluted concentration C_S of solute atoms S, can be expressed in terms of the self diffusion coefficient $D_A^\star(0)$, of the pure A matrix and the so called solvent enhancement factor $b_A^\star$ as,

$$D_A^\star(C_S) = D_A^\star(0)(1 + b_{A\star} C_S). \tag{53}$$

For bcc solvents $b_{A\star}$ is given by (28) while for fcc we adopt the expression in Ref. [24].

An important quantity that can be calculated from the phenomenological coefficients is the vacancy wind coefficient G, which provides essential information about the flux of S atoms induced by the vacancy flow. G is defined in terms of the Onsager coefficients as

$$L_{VS} = -(L_{SS} + L_{SA}) = -L_{SS}(G + 1). \tag{54}$$

Taking into account that $L_{SA} = L_{AS}$, we get the expression

$$G = \frac{L_{AS}}{L_{SS}}. \tag{55}$$

G in (55) accounts for the coupling between the flux J_A and J_S, through the vacancy flux, J_V [23]. It can be seen from (55) that If L_{VS} is negative ($G > -1$), solute and vacancy are moving in opposite directions, while, if L_{VS} positive ($G < -1$), a drag mechanism is dominant implying that vacancies and solutes are moving in the same direction [3,5,8]. The parameter G for fcc structures is calculated from the L-coefficients expressions, (16)–(18) and (31)–(38), for bcc and fcc lattices respectively.

5. Results

We present our numerical results to study the diffusion behavior in bcc and fcc *Fe*–*Cr* diluted alloys. Above the melting temperature $T_{\alpha\gamma} = 1183$ K, *Fe*–*Cr* alloys develop a paramagnetic fcc phase, while for lower temperature the structure is bcc. In this bcc phase, a magnetic transitions occurs from ferromagnetic, below the Curie temperature $T_C = 1043$ K, to paramagnetic states. In order to calculate the needed frequency jumps we used both CMS and DFT techniques coupled to the Monomer method [13].

As is usual, the vacancy formation energy (E_f^V) in pure *Fe* is calculated as,

$$E_f^V = E(N-1) + E_c - E(N), \tag{56}$$

where, $E(N)$ stands for the energy of the perfect lattice of N atoms, E_c is the cohesion energy and $E(N-1)$ is the energy of the defective system. For diluted alloys, we may consider the presence of the solute-vacancy complex $C_n = S + V_n$ in which, n = 1st, 2nd, 3rd, … (see Figs. 1 and 2) indicates that the vacancy is a n– nearest neighbors of the solute atom S. The binding energy between the solute and the vacancy for the complex $C_n = S + V_n$ is obtained as,

$$\begin{aligned} E_n^b &= \{E(N-2, C_n \\ &= Cr + V_n) + E(N)\} - \{E(N-1, V) + E(N-1, Cr)\}. \end{aligned} \tag{57}$$

In (57), $E(N-1, V)$ and $E(N-1, Cr)$ are the energies of a crystallite containing $(N-1)$ atoms of solvent *Fe* plus one vacancy V,

and one solute atom *Cr* respectively, while $E(N-2, C_n = Cr + V_n)$ is the energy of the crystallite containing $(N-2)$ atoms of *Fe* plus one solute vacancy complex $C_n = Cr + V_n$. With the sign convention used here $E_n^b < 0$ means an attractive solute-vacancy interaction, and $E_n^b > 0$ indicates repulsion.

The binding, formation and migration (E_m^V) energies were calculated with the Monomer method [13], a static technique to search the potential energy surface for saddle configurations. The Monomer computes the least local curvature of the potential energy surface using only forces. It must be mentioned that CMS simulations are much less computationally expensive method than DFT. When the Monomer is coupled to DFT calculations, the method is akin to the Dimer one from the literature [30], but roughly employs half the number of force evaluations which is a great advantage in ab-initio calculations.

The relaxation of impurities and defects, includes one substitutional *Cr* atom in *Fe*, as well as, a single vacancy. Current calculations have been performed at $T = 0$ K. In this case, the entropic barrier is ignored. Our calculations are carried out at constant volume, and therefore the enthalpic barrier $\Delta H = \Delta U + p\Delta V$ is equal to the internal energy barrier ΔU.

Classical calculations in bcc *Fe*–*Cr* were performed using the EAM potentials developed by Mendelev and Mishin [25]. For the fcc phase we use the EAM-13 potential developed by Bonny et al. [27]. Both EAM potentials reproduces well DFT results. We obtain the equilibrium positions of the atoms by relaxing the structure via the conjugate gradients technique. The lattice parameters that minimize the crystal structure energy are 2.8665 Å for bcc and 3.562 Å for fcc *Fe*–*Cr*. For all calculations we use a christallyte of $8 \times 8 \times 8$ containing 1024 (bcc) and 2048 (fcc) atoms, with periodic boundary conditions.

Quantum calculations were performed for the bcc phase using the open access SIESTA code [28]. Here, we assume spin polarization, a Mesh-CutOff parameter of 460 Ry, a smearing temperature of 0.15 eV (within a Fermi-Dirac scheme). The structure is relaxed when the forces are below 0.02 eV/Å. The basis sets for both elements consist in two and three localized functions for the 4s and 4p states, respectively, and five for the 3d states. The maximum cutoff radius is 5.1 Å. calculations were carried out with 54- and 128-atom supercells, using respectively a Brillouin zone sampling of $7 \times 7 \times 7$ and $4 \times 4 \times 4$ Monkhorst-Pack grid, and the Methfessel-Paxton broadening scheme with a 0.3 eV width. With this setup, we obtain a $T = 0$ K lattice parameter for bcc *Fe* of 2.885 Å. All calculations were performed using the GGA approximation for *Fe* and *Cr* [29,4].

In Table 3 we present our results for the formation and migration energies in pure bcc/fcc *Fe* from CMS and DFT calculations.

Binding and migration energies barriers, from CMS and DFT calculations, are shown in Tables 4 and 5 for both, bcc and fcc *Fe*–*Cr* alloys. Results reveal a weak repulsive/attractive energy interaction between the vacancy and solute for all calculations.

In order to obtain the frequency jumps from the calculated migration energies, we must first evaluate the pre-factor $\nu_0^\star$ in (45) which is calculated from (46). For this purpose, we calculate phonon frequencies under the harmonic approximation. As we already mentioned, the classical limit was employed for this calculation. Table 6 reports the calculated values of $\nu_0^\star$. Note that in Table 6 we report for the fcc *Fe*–*Cr* alloy, the same value of $\nu_0^\star$ as that for bcc *Fe*–*Cr* one.

From the values of E_m, in Tables 4 and 5, we calculate ω_i using equations (45) and (46) with $\nu_0^\star$ as reported in Table 6.

Once the jump frequencies in the multi-frequency model have been computed, the transport coefficients are calculated using analytical expressions in terms of the temperature.

Table 3
Energies and lattice parameters for pure bcc/fcc *Fe* from CMS and DFT calculations. The first column reports the employed method and some references. Second column specifies the simulation crystal, vacancy formation energy $E_f^V(eV)$ is shown in the third column. The forth column displays the migration energies E_m^V, calculated from the Monomer method [13]. In the fifth column we show the lattice parameter *a*. The last column displays the activation energy $E_Q(eV) = E_f^V + E_m^V$.

Reference	Fe_n	$E_f^V(eV)$	$E_m^V(eV)$	a(Å)	$E_Q(eV)$
		bcc-*Fe*			
Present work (CMS)	Fe_{1024}	1.72	0.68	2.8665	2.40
Chamati et al. [31]	Fe_{4500}	1.86	0.48	2.8665	2.34
Present work (DFT)	Fe_{54}	2.18	0.67	2.885	2.85
Present work (DFT)	Fe_{128}	2.05	0.68	2.885	2.73
SIESTA + drag method (DFT) [32]	Fe_{127}	2.18	0.69	2.885	2.87
Choudhury [5]	Fe_{54}	2.23	0.67	2.860	2.90
		fcc-*Fe*			
Present work (CMS)	Fe_{1024}	1.87	0.64	3.562	2.51
AKMC + NEB (DFT) [27]	Fe_{1024}	1.87	0.64	3.562	2.51

We calculate the solute correlation factors for bcc and fcc *Fe*–*Cr*, from (49) and (50). Results of f_{Cr} in terms of the inverse of the

Table 4
Binding and migration energies in bcc/fcc *Fe*–*Cr* with $N = 1024/N = 2048$ atoms calculated with CMS + Monomer [13]. The first column denotes the *Fe*–*Cr* structure. Binding energies E_n^b are shown in the second column. The third column describes the jump frequencies in Fig. 1. Migration energies E_m for direct and reversed jumps are written in the forth column. The last two columns show previous results for fcc *Fe*–*Cr* from DFT calculations [27] using the classical atomistic kinetic Monte Carlo (AKMC) method.

Lattice	$E_n^b(eV)$	ω_i	$E_m(eV)$	$E_n^b(eV)$	$E_m(eV)$
bcc	–	ω_0	0.68/0.68		
	0.04	ω_2	0.56/0.56		
	0.08	ω_3/ω_4	0.67/0.63		
	−0.003	ω_3'/ω_4'	0.56/0.60		
	−0.005	ω_3''/ω_4''	0.54/0.59		
	0.01	ω_5/ω_6	0.63/0.66		
	0.01	ω_7/ω_8	0.61/0.63		
	0.01	ω_7'/ω_8'	0.64/0.64		
fcc	–	ω_0	0.64/0.64		
	0.06	ω_1	0.66/0.66		
	0.06	ω_2	0.65/0.65	0.06*	0.65*
	0.01	ω_3/ω_4	0.76/0.72	0.01*	
	0.01	ω_3''/ω_4''	0.70/0.63		
	0.04	ω_3'/ω_4'	0.66/0.60		

Table 5
Binding and migration energies in bcc *Fe*–*Cr* with $N = 54$ and $N = 128$ atoms, using SIESTA + Monomer [13]. The Table description is he same as in Table 4. In columns 5–6, results taken from Refs. [4,5] using VASP with 54 atoms and SIESTA + Drag method with 128 atoms, respectively.

N	$E_n^b(eV)$	ω_i	$E_m(eV)$	$E_n^b(eV)$	$E_m(eV)$
	Present work			Ref. [5]	
54	–	ω_0	0.67/0.67	–	0.67/0.67
	−0.04	ω_2	0.57/0.57	−0.045	0.58/0.58
	0.01	ω_3/ω_4	0.67/0.64	−0.01	0.69/0.65
	0.01	ω_3'/ω_4'	0.63/0.61	−0.01	0.67/0.63
	0.09	ω_3''/ω_4''	0.60/0.59	−0.03	0.64/0.62
	−0.04	ω_5/ω_6	0.64/0.66	–	–
	Present work			Ref. [4]	
128	–	ω_0	0.68/0.68	–	0.69/0.69
	−0.04	ω_2	0.56/0.56	−0.04	0.57/0.57
	0.01	ω_3/ω_4	0.67/0.63	–	0.64/0.66
	0.01	ω_3'/ω_4'	0.60/0.60	–	0.69/0.65
	0.09	ω_3''/ω_4''	0.58/0.59	–	0.67/0.66
	−0.04	ω_5/ω_6	0.63/0.65	–	0.74/0.74

temperature, are shown in Fig. 3.

Fig. 4 shows that $b^{\star}_{Fe}$ is positive in all the temperature range and increase monotonically with $1/T$ for the bcc *Fe–Cr* alloy, while is negative for fcc *Fe–Cr*. This difference will be highly diminished in the diffusion coefficient because the enhancement factor is multiplied by the solute concentration C_S, which is low for diluted alloys.

In the framework of a random alloy model, Belova and Murch [37,38], have studied the enhancement of the solvent diffusivity, as well as, the solvent correlation factor in diluted binary alloys in terms of the jump frequencies ω_i. The authors have performed an extensive Monte Carlo study of the tracer correlation factors in simple cubic, bcc and fcc binary random alloys. On the other hand, the kinetic formalism of Moleko et al. [39], also describes the behavior of the tracer correlation factors for slow and faster diffusers.

In the case of CMS calculations, the Onsager and diffusion coefficients were obtained by assuming a solute mole fraction of $C_S = 0.001$, which corresponds to $n_{Cr} = 8.59 \times 10^{25}\ m^{-3}$ at. and $n_{Cr} = 8.85 \times 10^{25}\ m^{-3}$ at., respectively for bcc and fcc *Fe–Cr*. For DFT calculations, with $N = 54$ and $N = 128$ atoms, we assume a solute molar fraction of $C_S = 0.01$ and $C_S = 0.001$, respectively.

Once the Onsager coefficients L_{AS} and L_{SS} are obtained, the vacancy wind coefficient $G = L_{AS}/L_{SS}$ can be calculated directly from (55). CMS and DFT results are presented in Fig. 5. We see that $G > -1$ for all the temperature range considered, showing that the vacancy drag mechanism is unlikely to occur in both bcc and fcc phases using the present description. Our results are in agreement with those in Refs. [5,33].

The full set of *L*-coefficients are displayed in Fig. 6 against $1/T$, T in *K*. We see that the *L*-coefficients follow an Arrhenius behavior, which implies in a linear relation between the logarithm of *L*-coefficients against the inverse of the temperature (see Fig. 6).

Now, we are in position to obtain the diffusion coefficients $D^{\star}_A$, $D^{\star}_S$. First, we present the ratio of the calculated tracer diffusion coefficients $D^{\star}_S/D^{\star}_A$ as a function of the inverse of the temperature in Fig. 7.

The ratio of the tracer diffusion coefficients is particularly important to understand the Radiation Induced Segregation (RIS) profile in the *Fe–Cr* system. The ratio of transport coefficients which determines the sign of RIS is the ratio $C_A(L_{SS} + L_{AS})/C_B(L_{AA} + L_{AS})$ and the ratio $D^{\star}_S/D^{\star}_A$ is an approximation of the latter. In comparison with experimental data in Ref. [5] in Fig. 4b, our CMS and DFT calculations accurately predict the relative relationship of tracer diffusion coefficients between *Fe* and *Cr* in the ferromagnetic *Fe* phase where the quotient is around 1.3–1.8.

In Figs. 8–10, we show the calculated $D^{\star}_S$ and $D^{\star}_A$ using equations (48) and (53), respectively. For the solute correlation factor, f_S, we discriminate between bcc and fcc *Fe* using expressions in (49) and (50), while for f_0, we use the associated values $f_0 = 0.7272$ and $f_0 = 7814$, respectively (see Section 4). We compare present calculations with reliable experimental data which were plotted in black triangles for *Fe* and orange stars for *Cr* (color online).

The present model is improved when the magnetic order is taken into account and the phonon spectrum is used to compute the mean jump frequencies involved in the tracer diffusion coefficients. In this way, it is important to consider the study of Self-diffusion in bcc iron by Iijima et al. [34], using a serial radio-frequency sputter-microsectioning method with radioactive tracers ^{55}Fe and ^{59}Fe in the temperature range 766–1148 K. Above the Curie temperature the self-diffusion coefficient shows a linear Arrhenius relationship with negligible influence of the short range magnetic spin ordering, while below the Curie temperature $T_C = 1043$ K, temperature dependence of the self-diffusion coefficient deviates from the linear Arrhenius relationship due to spontaneous magnetization. The temperature dependence of the self-diffusion coefficient, $D^{\star}_A$, in the whole temperature range of bcc *Fe* across the Curie temperature, has been expressed by

$$D^{\star}_X = D^{\star}_X(0)\exp\left\{-\frac{Q^P_X[1+\alpha_X s^2_X(T)]}{k_B T}\right\}\mathrm{m^2 s^{-1}}, \tag{58}$$

where $X = S$ or A respectively for the solute or solvent atom, $Q^P_A = E^V_f + E^V_m$ and $Q^P_S = E^V_m + E^V_f + E_b$. $s_A(T)$, $s_S(T)$ are the ratio of the spontaneous magnetization at TK to that at 0 K [35], and $s_A(T) = s_S(T) = 1$ in the full temperature range of the ferromagnetic phase. In (58) the activation energies in the paramagnetic phase is corrected by the spontaneous magnetization term. Here we extrapolate the values of $\alpha_{Fe}s(T)$ and $\alpha_{Cr}s(T)$ in Ref. [35] using a quadratic curve from Ref. [36].

The modified activation energy is used in calculating the tracer diffusion coefficients, as previously in the calculations of the Onsager coefficients. The tracer diffusion expressions in Eqs. (47) and (52) are partitioned into pre-exponential factors and activation energies to match the Arrhenius form following the procedure in Ref. [5].

Fig. 8 shows the CMS calculations in two approximations. Fig. 8 (Left panel), shows the CMS calculated values of $D^{\star}_A$ and $D^{\star}_S$ using, as in Ref. [5], $\nu^{\star}_0 = 5 \times 10^{12}$ Hz and neglecting magnetic order corrections to the activation energy. In the right panel, we show, the here improved model, using the calculated phonon spectrum to compute $\nu^{\star}_0$ (as in Table 6) involved in ω_i's, as well as, assuming magnetic corrections to the paramagnetic *Fe* phase using eq. (58) for self and solute activation energies.

We have observed that, the use of a different value of $\nu^{\star}_0$ shifts "rigidly" the diffusion profile without changing the overall shape. The change of shape in Fig. 8 from left to right panels is due to magnetic corrections that are taken into account in the right panel and not in the left one. This is the reason why in the left panel (with no magnetic corrections) the slopes for the bcc paramagnetic and ferromagnetic phases are the same, there is no trace of the phase transition. While in the right panel, the phase transition is clearly seen by the change in the slope, which is due to the magnetic correction taken into account for the ferromagnetic phase.

We can then observe that, for our improved model, Fig. 8 right panel, calculations are in very good agreement with the experimental data measured in Refs. [34,36], for both the solvent and solute diffusion coefficients.

Fig. 9, shows our results from DFT calculations with 54 (Left) and 128 (Right) atoms with the above described improved model. That is, taking into account, for both panels, magnetic corrections for the ferromagnetic phase, as well as the calculation of $\nu^{\star}_0$ from the phonon spectrum. We can then observe that the slope of the results of DFT calculations are in agreement with experimental data, however the absolute value has a gap which is reduced by increasing the total number of atoms as is shown in comparing Fig. 9 left panel (54 atoms) with right panel (128 atoms). Also, it can be seen that, although a better agreement with experimental data

Table 6
Attempt frequencies $\nu^{\star}_0$ in (45) from CMS calculations, in units of the Debye value $\nu_D = 10^{13}$ *Hz* [4].

Reference	Lattice	*Fe* → *V* in *Fe*	*Cr* → *V* in *Fe*
Present work	bcc	10.9	9.8
Ref. [4]	bcc	8.17	8.17
Present work	fcc	10.9	9.8

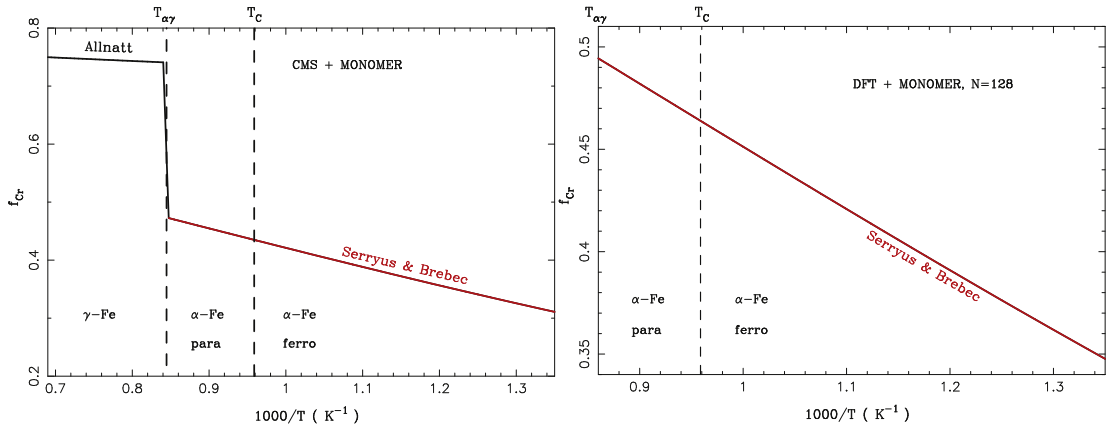

Fig. 3. Solute correlation factor, f_{Cr}, from CMS (Left) and DFT (Right) calculations *vs* $1/T$.

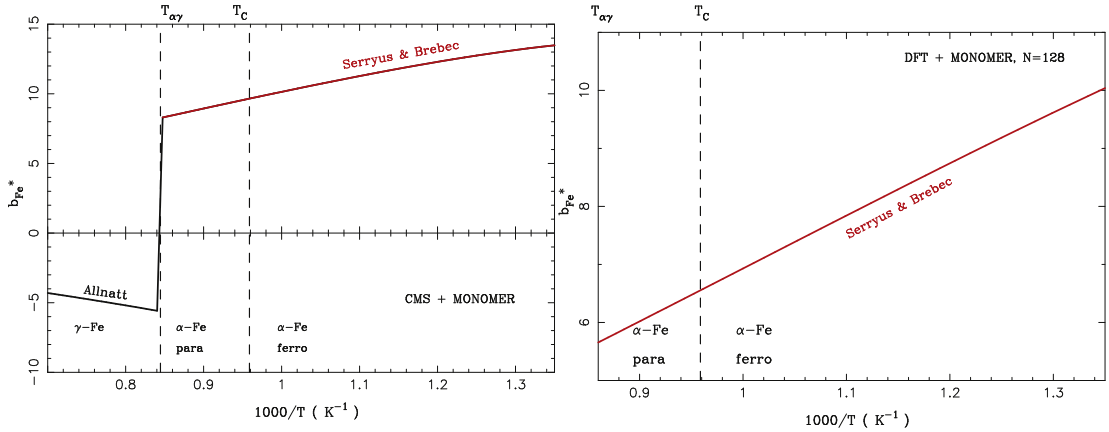

Fig. 4. Solvent-enhancement factor, b_{Fe}, from CMS (Left) and DFT (Right) calculations *vs* $1/T$.

is observed when the number of atom is increased, CMS simulations, shown in Fig. 8 (right panel), give more accurate results than DFT ones.

In addition, in Fig. 10, we show the diffusion coefficients obtained with DFT calculation with 54 atoms taking into account the magnetic corrections, but using, as in Ref. [5], $\nu_0^\star = 5 \times 10^{12}$ Hz. That is, without taking into account the calculated phonon spectrum to compute $\nu_0^\star$. In comparison with Fig. 9 left panel, the use of a different value of $\nu_0^\star$ which shifts "rigidly" the diffusion profile without changing the overall shape, as we already mentioned.

Our calculations in Fig. 10, reproduce the results in Ref. [5]. We can then observe that, although the slope of the diffusion coefficients *vs* $1/T$ matches well with experimental measurements, the absolute value differs in four orders of magnitude.

Hence, the discrepancy between the measured and calculated tracer diffusion coefficients, reported in Ref. [5], arises from two features. The effect of the contributions of the phonon vibrations as been neglected for the calculation of the frequency jumps. On the

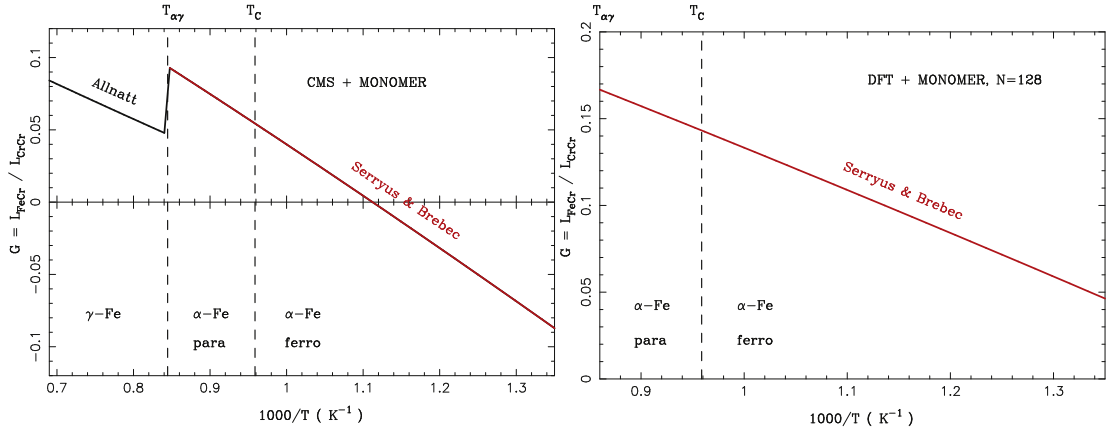

Fig. 5. The vacancy wind coefficient G in (55) from CMS (Left) and DFT (DFT) methods.

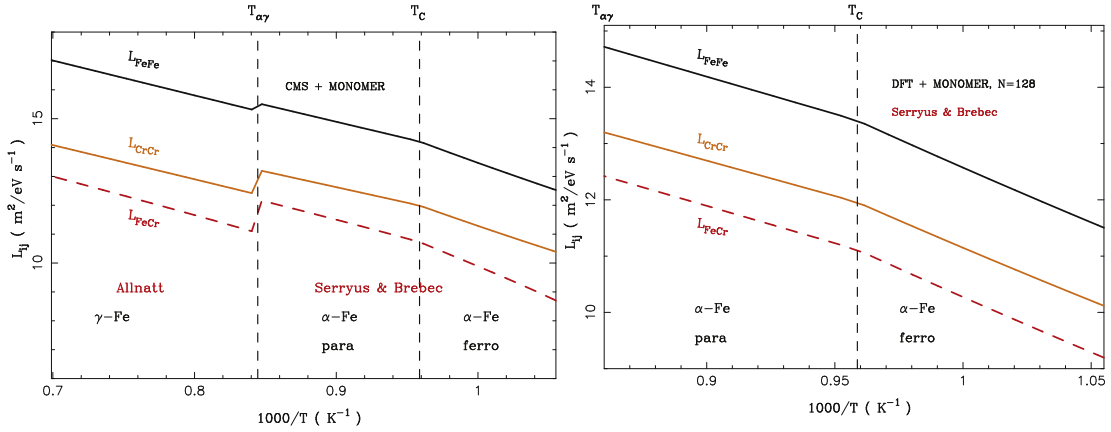

Fig. 6. Onsager phenomenological coefficients from CMS (Left) and DFT (Right) calculations *vs* $1/T$.

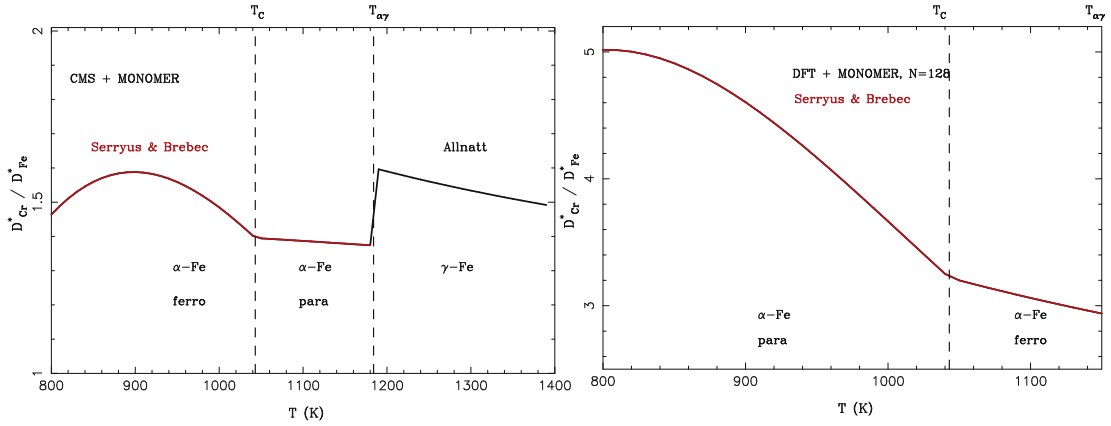

Fig. 7. Ratio of the tracer diffusion coefficient $D_S^\star/D_A^\star$ *vs* $1/T$ from CMS (Left) and DFT (Right) calculations.

other hand, the use of ab-initio calculations with a too small number of atoms can deliver incorrect results.

On the other hand, a similar accordance with experimental data have been obtained using also a classical model, namely classical Kinetic Monte Carlo algorithm with temperature dependent pair interactions [4].

In Ref. [26], it was found that self-diffusion in pure bcc *Fe* is controlled by the vacancy mechanism at all temperatures. The authors have obtained good agreement of the calculated diffusivity with experimental data.

In summary, our present calculations for diluted alloys using both, CMS and DFT, confirm that a vacancy drag mechanism is unlikely to occur in bcc/fcc *Fe*–*Cr* diluted alloys, in agreement with previous results in Ref. [5]. The full set of *L*-coefficients against $1/T$,

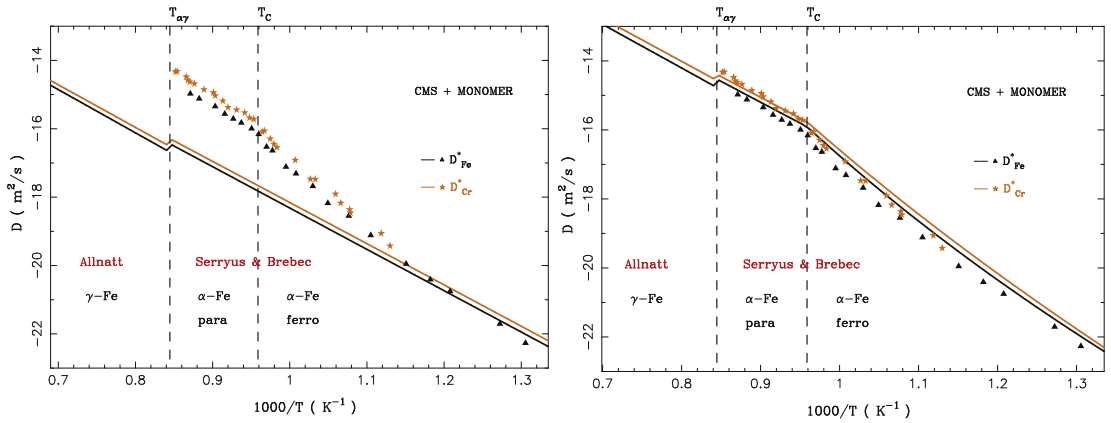

Fig. 8. Tracer self and *Cr* diffusion coefficients in *Fe*–*Cr* from CMS calculations. Left: Using, as in Ref. [5], $\nu_0^\star = 5 \times 10^{12}$ Hz and neglecting magnetic order corrections to the activation energy. Right: Using $\nu_0^\star$ calculated phonon spectrum (as in Table 6) and magnetic correction to the ferromagnetic bcc-*Fe* phase. The lines correspond to the present model, while stars and triangles correspond to the experimental values from Refs. [34,36], for *Fe* and *Cr*, respectively.

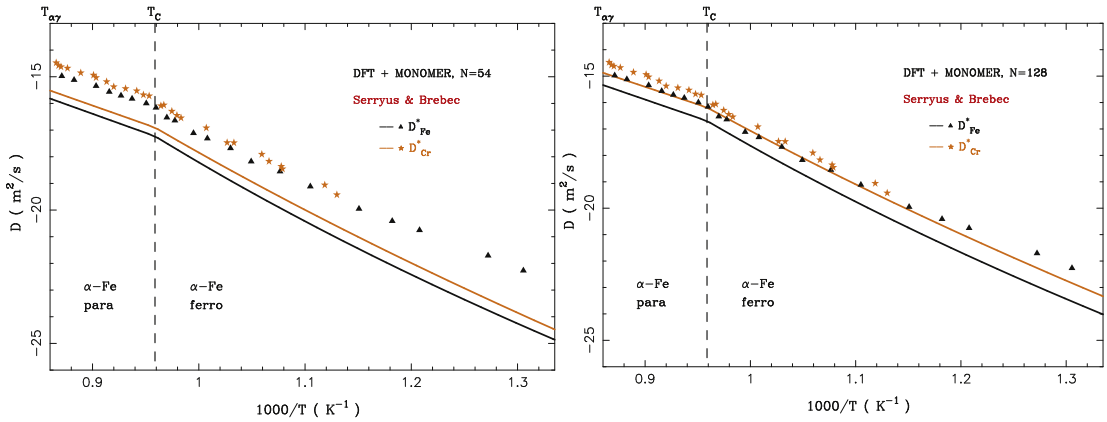

Fig. 9. Self-diffusion and *Cr* diffusion coefficients in *Fe–Cr* from DFT calculations with N = 54 (Left) and 128 (Right) atoms including magnetic correction to the paramagnetic bcc-*Fe* phase.

with magnetic order corrections, follow an Arrhenius behavior. On the other hand, present calculations from CMS, are in very well agreement with experimental values of $D_A^{\star}$ and $D_S^{\star}$.

Finally we want to mention that, Garnier et al. [40], have investigated the drag of solute atoms by vacancies at low temperatures, using a self-consistent mean field method. The method takes into account interactions between the solute atom and a vacancy up to the third nearest neighbor sites. They have identified the mechanism involved in the solute drag by vacancies. Then, it would be interesting to extend the calculations for a twelve-frequency model as in Ref. [40] in order to obtain convergent results independently of the approximation employed.

6. Concluding remarks

In summary, in this work the diffusion properties in *Fe–Cr* diluted alloys have been studied in an important temperature range that includes both para and ferro magnetic orders as well as bcc and fcc structures. For our study, we have adopted a multi frequency model where the migration is driven by a vacancy mechanism. The present model is improved when the magnetic order is taken into account and the phonon spectrum is used to compute the mean jump frequencies involved in the tracer diffusion coefficients.

The flux equations connect the diffusion coefficients with the Onsager tensor. While kinetic theory allows to write this Onsager coefficients in terms of jump frequencies. In this way we could write expressions for the diffusion coefficients only in terms of microscopic magnitudes, i.e. the jump frequencies. In this context, we use the approach developed by Allnatt [10,11] and Serryus and Brevec [7] for fcc and bcc solvent phases, respectively. The multi-frequency model has also been of great utility in order to discriminate the relevant jump frequencies, which have been calculated thanks to the economic technique namely the Monomer.

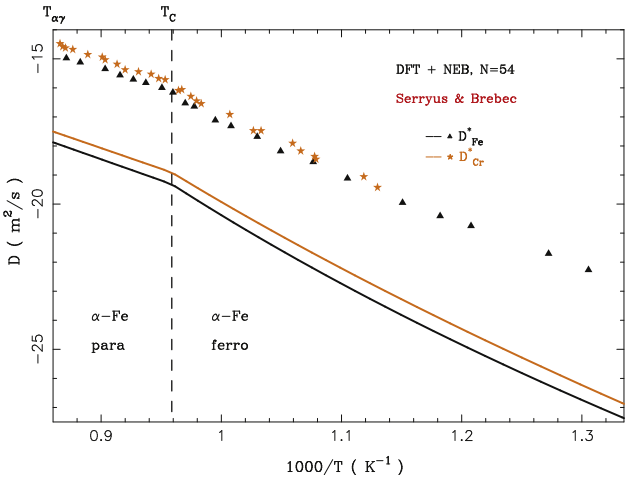

Fig. 10. Self-diffusion and *Cr* diffusion with DFT calculation with 54 atoms taking into account the magnetic corrections, but using, as in Ref. [5], $\nu_0^{\star} = 5 \times 10^{12}$ Hz.

For the bcc phase, we have performed our calculations using both, CMS as well DFT calculations with 54 and 128 atoms. Although, DFT based results, depends on the size of the atomic cell, CMS results do not. This is a consequence of quantum coherence, that only DFT calculations take into account. In this way, our calculations show that, in accordance with Bohr's correspondence principle, as the size of the atomic cell (total number of atoms) is increased, quantum results with DFT recover the classical ones obtained with CMS.

On the other hand, temperature destroys coherent effects, and the atomic diffusion process is studied at temperatures much higher than ambient. In that case, the interaction of the system with the thermal environment implies in decoherence effects, where the classical limit is expected to be recovered. Hence, we do not expect to observe any quantum feature.

Indeed, our results obtained with CMS simulations are in very good agreement with available experimental data for both, tracer solute and solvent diffusion coefficients. A similar accordance with experimental data have been obtained using also a classical model, namely classical Kinetic Monte Carlo algorithm with temperature dependent pair interactions [4]. It must be noted that, the agreement between CMS calculation and experimental data is not fortuitous, it have been recently observed for diffusion in *Ni–Al* and *Al–U* fcc lattices [3]. Hence, the atomic diffusion process in metals is a classical phenomena, for which the large number of atoms and the temperature has suppressed any coherent effect. Then, if reliable semi empirical potentials are available, a classical treatment of the atomic transport in metals is much convenient than DFT.

In addition, the accordance with experiments validates the here used multi frequency model. This implies that the diffusion process, at thermal equilibrium, is mainly due to a vacancy mechanism. It must be also noted that CMS simulations are much less computationally expensive method than DFT, for which computational time largely increases with the number of atoms of the quantum sample to be simulated.

For high temperatures, in the fcc phase, only CMS calculations where performed. In that case, no experimental date of diffusion

coefficients have been yet reported for *Fe–Cr* diluted alloys. Then, our CMS calculations predict the diffusion behavior in this fcc phase. Also the present CMS and DFT calculations in both bcc and fcc phases, reveal that *Cr* in *Fe*, at diluted concentrations, migrates as free species which implies that a vacancy drag mechanism is unlikely to occur within the present approach.

Acknowledgments

We are grateful to Dr. Roberto C. Pasianot for valuable discussions. This work was partially financed by CONICET PIP-00965/2010 and CNEA/CAC – Gerencia Materiales.

References

[1] C. Hurtado Noreña, P. Bruzzoni, Mater. Sci. Eng. A (2010) 410–416.
[2] P. Castaño Rivera, V.P. Ramunni, P. Bruzzoni, Corros. Sci. 54 (2012) 106–118.
[3] Viviana P. Ramunni, Comp. Mater. Sci. 93 (2014) 112–124.
[4] E. Martínez, O. Senninger, C.C. Fu, F. Soisson, Phys. Rev. B 86 (2012) 224109.
[5] S. Choudhury, L. Barnard, J.D. Tucker, T.R. Allen, B.D. Wirth, M. Asta, D. Morgan, J. Nucl. Mater. 411 (1–3) (2011) 1–14.
[6] A.D. Le Claire, J. Nuc. Mater. 69 & 70 (1978) 70–96.
[7] Y. Serruys, G. Brebec, Philos. Mag. A 46 (1982) 661.
[8] J.D. Tucker, R. Najafabadi, T.R. Allen, D. Morgan, J. Nucl. Mater. 405 (2010) 216–234.
[9] M. Mantina, Y. Wang, L.Q. Chen, Z.K. Liu, C. Wolverton, Acta Mater. 57 (2009) 4102–4108.
[10] A.R. Allnat, J. Phys. C. Solid State Phys. 14 (1981) 5453–5466.
[11] A.R. Allnat, J. Phys. C. Solid State Phys. 14 (1981) 5467–5477.
[12] G.H. Vineyard, J. Phys. Chem. Solids 3 (1957) 121.
[13] V.P. Ramunni, M.A. Alurralde, R.C. Pasianot, Phys. Rev. B 74 (2006) 054113.
[14] R.C. Pasianot, R.A. Pérez, V.P. Ramunni, M. Weissmann, J. Nucl. Mater. 392 (1) (2009) 100–104.
[15] V.P. Ramunni, R.C. Pasianot, P. Bruzzoni, Phys. B 404 (18) (2009) 2880–2882.
[16] V.P. Ramunni, C. Hurtado-Noreña, P. Bruzzoni, Phys. B Condens. Matter 407 (16) (2011) 33013304.
[17] A.R. Allnatt, A.B. Lidiard, Atomic Transport in Solids, Cambridge University Press. Ed, 2003.
[18] G.E. Murch, Z. Qin, Defect Diffusion Forum 109 (1994) 1–18.
[19] Z. Qin, G.E. Murch, Philos. Mag. A 67 (1993) 757.
[20] J.R. Manning, Phys. Rev. 136 (1964) A175846.
[21] M. Koiwa, S. Ishioka, Philos. Mag. A 47 (1983) 927.
[22] K. Toyoura, Y. Koyama, A. Kuwabara, F. Oba, I. Tanaka, Phys. Rev. B 78 (2008) 214303.
[23] J.L. Bocquet, G. Brebec, Y. Limoge, Diffusion in Metals and Alloys, Elsevier Science BV, Amsterdam, The Netherlands, 1996, p. 535.
[24] J.L. Bocquet, Acta Metall. 22 (1974).
[25] M.I. Mendelev, S. Han, D.J. Srolovitz, G.J. Ackland, D.Y. Sun, M. Asta, Philos. Mag. 83 (2003) 3977.
[26] M.I. Mendelev, Y. Mishin, Phys. Rev. B 80 (2009) 144111.
[27] G. Bonny, N. Castin, D. Terentyev, Model. Simul. Mater. Sci. Eng. 21 (2013) 085004.
[28] J.M. Soler, E. Artacho, J.D. Gale, A. Garcia, J. Junquera, P. Ordejón, D. Sanchez-Portal, J. Phys. Condens. Matter 14 (2002) 2745.
[29] E. Martinez, C.-C. Fu, Phys. Rev. B 84 (2011) 014203.
[30] G. Henkelman, H. Jónsson, J. Chem. Phys. 111 (2002) 15. Surfaces, interfaces, and materials.
[31] H. Chamati, N.I. Papanicolaou, Y. Mishin, D.A. Papaconstantopoulos, Surf. Sci. (2006) 1793–1803.
[32] C.C. Fu, F. Willaime, P. Ordejón, Phys. Rev. Lett. 92 (2004) 175503.
[33] L. Messina, Z. Chang, P. Olsson, Nucl. Instrum. Methods Phys. Res. B 303 (2013) 28–32.
[34] Y. Lijima, K. Kimura, K. Hirano, Acta Metall. 36 (10) (1988) 2811–2820.
[35] J. Crangle, G.M. Goodman, Roy. Soc. Lond. Ser. a-Math. Phys. Sci. 321 (1971).
[36] C.G. Lee, Y. Iijima, T. Hiratani, K.I. Hirano, Mater. Trans. JIM 31 (1990) 255.
[37] I.V. Belova, G.E. Murch, Philos. Mag. A 80 (7) (2000) 1469–1479.
[38] I.V. Belova, G.E. Murch, Philos. Mag. A 83 (3) (2003) 393–399.
[39] L.K. Moleko, A.R. Allnatt, E.L. Allnatt, Philos. Mag. A 59 (1989) 141.
[40] T. Garnier, M.S. Nastar, P. Bellon, D. Trinkle, Phys. Rev. B 88 (2013) 134201.